Theoretical investigation of the van der Waals interaction in Ba$^{0,+,2+}$He systems and the stability of Ba^{2+}He$_n$ clusters

Héla Habli[1,2], Soulef Jellali[1], Mtiri Safa[1] 🟢 and Brahim Oujia[3]

[1] Université de Monastir, Faculté des Sciences de Monastir, Laboratoire de Physique Quantique et Statistique, Avenue de l'Environnement 5019, Monastir, Tunisie
[2] Université de Sousse, Institut Supérieur des Sciences Appliquées et de Technologie de Sousse, Rue ibn Khaldun, Cité Taffala, 4003 Sousse, Tunisie
[3] University of Jeddah, Faculty of Science, Physics Department, Jeddah, Saudi Arabia

E-mail: hablihela@gmail.com

CrossMark

Abstract

An *ab-initio* calculation was performed to highlight the van der Waals interaction between Ba$^{0,+,2+}$ and helium atoms. The low-lying electronic states for Ba$^+$He and BaHe systems have been determined with the ECP-CPP and full valence CI theory. However, the core-core interaction for Ba^{++}He has been calculated by the CCSD(T). As a result, the spectroscopic parameters and the vibrational levels have been derived from Potential Energy Surface (PES) and compared with available theoretical and experimental data. Then, the permanent dipole moments for the ground and the excited states are determined. These results show an important shape in PES and allow checking the strong repulsive interactions between Rydberg electrons and the He atom. Furthermore, structures and stabilities of the Ba^{++}He$_n$ mixed-clusters have been investigated by exploring the PES based on the BHMC algorithm. The most stable icosahedral structure was detected at n = 12 and the snowball shell was completed at n = 20.

Keywords: potential energy surface, vibrational level, dipole moment, Ba^{++}He$_n$ clusters, global optimization

(Some figures may appear in colour only in the online journal)

1. Introduction

Alkaline-earth (AE) ions and free electrons immersed in condensed helium have a significant role in many areas such as biochemistry, quantum physics, astrophysics and biomolecular sciences [1–16]. Kanorsky groups [5, 6] reported an experimental study of laser excitation and fluorescence spectra of barium atoms in superfluid helium. Their studies were focused on the transition {6s^2 (^{1}S$_0$) → 6s6p (^{1}P$_1$)} at 1.5 K, for which the shift of the excitation and emission lines were explained and measured. Additionally, experimental and computational closed-shell interactions Ba^{2+} with RG atoms (RG = He to Xe) were carried out by Koyanagi *et al* [16]. In Selected Ion Flow Tube Mass Spectrometer (SIFT-MS) at room temperature, these authors showed exceptional observations for the formation of diatomic molecules BaRG^{2+} in

helium bath gas. They explained that the interaction force between Ba^{2+} and RG, and also the rate of formation of BaRG^{2+} increase with increasing RG polarizabilities. In 2011, Lebedev groups [14] used the optical spectroscopy to study the fluorescence relaxation of barium cations in condensed helium. They proved that the ^{3}D$_1$ metastable state can be used as an intermediated state in two-step excitations of high-lying states. More recently, barium cation immersed in superfluid He is investigated by Batulin and coworkers [1]. They observed the Laser-Induced Fluorescence (LIF) of Ba$^+$ injected into liquid ^{4}He by the plasma of radiofrequency discharge in Ba-He gas. Furthermore, excitation of barium with helium liquid as well as with argon clusters was used as an indicator for solvation effects in different studies [1, 4, 5, 7].

On the other hand, the transport properties of barium atom and its cation with rare gas are the subject of various works [2, 3, 17–19]. For barium cation, these properties have been calculated as a function of $\frac{E}{n_0}$ in drift tubes filled with helium and argon buffer gases [17–20], where E is the electrostatic field strength and n_0 represent the gas number density. Following to the gas-phase studies, the mobility of Ba^+ in superfluid ^4He, in the temperature range from 1.27 to 1.66 K, has been determined by Foerste and coworkers [21]. In 2009, McGuirk *et al* [3] investigated the potentials of the Ba^+RG and $Ba^{2+}RG$ (RG = He to Rn) at the RCCSD(T) level. They employed, for Ba ions, a 46-electron ECP with a particular basis set aug-cc-pV5Z. Then, they used these potentials to obtain the transport coefficients for Ba^+ and Ba^{2+} moving through a RG bath. Thereafter, Buchachenko *et al* [2] calculated the ground states potentials for $Ba^{m+}RG$ complexes (m = 0, 1, 2; RG = He to Xe) with the CCSD(T) method. They have determined the collision cross sections and the transport coefficients.

Several theoretical works [2, 3, 22–31] were devoted to the interaction potentials for the ground state of the Ba^{m+} in rare gas complexes. As an example, Abdessalem and co-workers [29] investigated the many-body effects on the structures and the stability of $Ba^{2+}Xe_n$ (n = 1–34) clusters. The first shell is closed for n = 12 corresponding to icosahedral geometry. Afterward, Issa *et al* [28] studied the $Ba^{2+}Ar_n$ system by the employing of pair-wise interaction. They predicted that stable geometries are based on icosahedral packing. For n = 18, n = 22, and n = 25, they obtained the double, triple and quadruple icosahedrons geometries, respectively. In 2018, Tuttle *et al* [30] provided deep insight into the nature of the bonding of metal cation/rare gas complexes. Recently, Bezrukov and coworkers [31] investigated a set of the *ab initio* potentials for the complexes Ba/Ba^+ with rare gas (Ar, Kr, Xe) in the states related to the $6s \rightarrow 5d$ and $6s \rightarrow 6p$ excitations.

Furthermore, the interaction potentials between alkaline-earth and helium investigated by several groups [5, 26, 30, 32–46]. Breckenridge and coworkers calculated the PES for the $He-Mg^{0,+,2+}$ van der Waals complexes [41]. They concluded that the ion/induced-dipole interaction of the Mg^{2+}/He core is the main attractive force in $^3\Sigma^-$, $^2\Pi$ and $^3\Sigma^+$ states dissociating into $Mg(3p\pi3p\pi)-He$, $Mg^+(3p\pi)-He$, and $Mg^{2+}(2p^6)-He$ limits, respectively. Sapse and coworkers [43] studied the X^+He_n (X = Li, Na, Mg) complexes at the MP2/6–311 + G(3df, 3pd) level. They showed that the bent geometry is the most stable. Lovallo *et al* [33, 37] proved the existence of three bound rovibrational states for each MHe system. In 2004, Bu and coworkers [44, 45, 47] studied the Be^+He_n and $Mg^{+,2+}He_n$ complexes at the HF, MP2, and MP2(full)/6–311 + G(3df,3pd) levels. They showed that the $Mg^{2+}He_n$ are more stable than the Mg^+He_n complexes, and their first solvation shells are formed by 9and 20 helium atoms, respectively.

Spectroscopic properties of the ground and excited states of $MgHe_n$ through the MP4, CCSD, and CCSDT levels have

been presented in the [34] and a good agreement with the experimental cluster spectra have been shown. In 2008, Page and von Nagy-Felsobuki [48] studied the $Mg^{2+}He_2$ and $Ca^{2+}He_2$ complexes using the *ab initio* calculation at the CCSD (T), IC-MRCI and IC-MRCI + Q levels. They found that the $Mg^{2+}He_2$ was linear structure while the $Ca^{2+}He_2$ was a quasi-linear structure. For size 2, there are complexes with linear and others with bent structure, which can be shown in terms of repulsive and attractive forces as well as the hybridization processes [49].

A review of the literature shows that few calculations have been performed on $Ba^{m+}He$ (m = 0, 1, 2) van der Waals system and there is no experimental information about the geometric structures of $Ba^{++}He_n$ complexes accessible. The purpose of the present work is to report on a comprehensive *ab initio* study for different states of van der Waals interaction in $Ba^{0,+,2+}$ He systems and also for the stability of $Ba^{++}He_n$ clusters.

We start our computational approach with the determination of the core-core interaction potential energy at the CCSD (T) level and the electronic energy interaction between valence electron and $Ba^{++}He$ ionic system. Second, we calculate the PES, spectroscopic constants, vibrational levels and electric dipole moments associated with several symmetries. Then, we update the comparisons with current experimental and theoretical data found only in the ground state of the $Ba^{m+}He$ systems. Third, we investigate the stable geometries by exploring the potential energy surface using the basin-hopping global optimization technique for the $Ba^{2+}He_n$ clusters.

2. Theoretical background

2.1. Ab initio calculation

The total potential (V_{tot}) for the alkaline-earth rare gas $M^{m+}RG$ systems is the sum of the core-core interaction potential ($V_{M^{++}-RG}$) and the electronic interaction between the valence electron '*ve*' and the ionic system $M^{++}RG$ ($V_{ve-M^{++}RG}$). In this context:

(i) The core-core interaction ($V_{Ba^{++}-He}$), corresponding to the interaction between the Ba^{++} core and the helium atom, is calculated by using the Coupled Clusters with the iterative treatment of the Single and the Double excitation amplitudes and the perturbative treatment of triples (CCSD(T)) theory as incorporated in the Molpro software [50]. For the helium atom, we used the standard aug-cc-pV5Z basis set [51]. We employed an effective core potential ECP (ECP46MDF [52]) with the valence aug-cc-pV5Z basis set [53] for the barium atom.

The spectroscopic parameters for the Ba^{++}-He potential are extracted and listed in table 1, with those found in other published works [2, 3, 35, 54, 55]. We can clearly observe a good agreement for the

Table 1. Spectroscopic constants compared with the available results for Ba^{++}He complex. (Equilibrium bond length R_e; Dissociation energies D_e; Harmonic frequency ω_e; anharmonic constant $\omega_e\chi_e$; Rotational constant B_e).

R_e (a.u.)	D_e (cm^{-1})	ω_e (cm^{-1})	$\omega_e\chi_e$ (cm^{-1})	B_e (cm^{-1})
5.47	558	142.7	9.3	0.515
5.40[a]	603.7[a]	175.2[a]	17.4[a]	0.505[a]
5.37[b]	637.6[b]	175.7[b]	14[b]	0.542[b]
5.00[c]	950[c]	—	—	—
4.92[d]	880[d]	—	—	—
5.36[e]	638[e]	176[e]	—	—

[a] [2];
[b] [3];
[c] [35];
[d] [54];
[e] [55].

Figure 1. Comparison between the calculated CCSD(T) (black line) potential energy surface for Ba^{++}He interaction and the Tang and Toennies analytical potential (Symbol line).

equilibrium bond length as well as for the well depth with the Buchachenko *et al* [2], where their differences are 0.07 a.u and 45.7 cm^{-1}, respectively. We note a small difference in the well depth with those found by Brust *et al* [54] and Czuchaj *et al* [35].

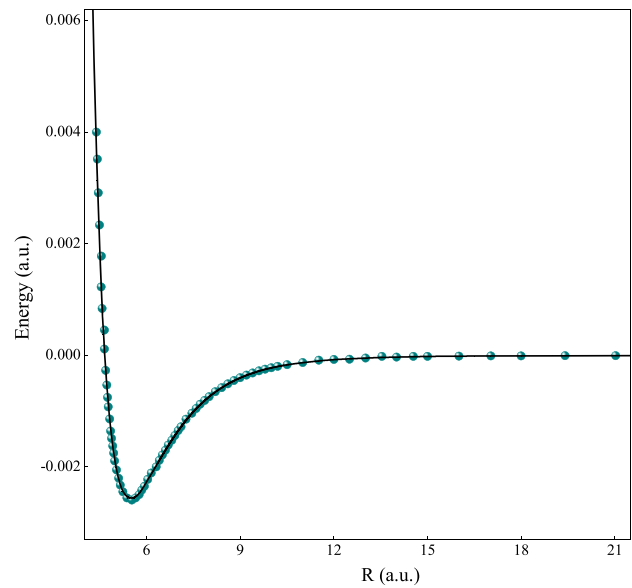The accuracy obtained for the potential energy of the Ba^{++}He is crucial for better representation of electronic states for ionic and neutral systems (Ba$^+$He, BaHe). In this case, the potential for the Ba^{++}-He interaction has been fitted using the analytical form of Tang and Tonnies [56] which is expressed as follow:

$$V(r) = A\exp(-b\,r) - \left(\frac{C_4 \times \alpha_{He}}{2\,r^4}\right) - \left(\frac{C_6}{r^6}\right) - \left(\frac{C_8}{r^8}\right) - \left(\frac{C_{10}}{r^{10}}\right)$$

The first term in this potential describes a repulsive exponential dominating at short-range. The second term is the helium polarization contribution. The remaining terms express the long-range dispersion interactions (dipole-dipole, dipole-quadrupole, quadrupole-quadrupole). The parameters A, b, C_4, C_6, C_8 and C_{10} result from the square fitting of the numerical potential. The $\alpha_{He} = 1.383\,a_0^3$ [57] is the helium's polarizability. The obtained parameters are in a.u: $A = 14.4025$, $b = 1.467$, $C_4 = -4.3743 \quad 10^{-6}$, $C_6 = 233.05$, $C_8 = -24.42$, $C_{10} = -33905$.

Figure 1 displays the numerical potential of Ba^{++}-He compared to the analytical one, where the maximal deviation between them for all internuclear distances does not exceed 5 cm^{-1}.

(ii) The electronic energy interaction between valence electron and ionic system Ba^{++}He resulting from *ab-initio* calculations ($V_{ve-Ba^{++}He}$) is determined by the full valence CI theory including the CPP and ECP approaches. Therefore, the Ba$^+$He and the BaHe systems are treated as one and two active electron systems, respectively, where the core electrons of barium and helium atoms are replaced by pseudo-potentials. The

core-valence correlation is described by the following effective potential [58]:

$$V_{cpp} = -\frac{1}{2}\sum_c \alpha_c\,\vec{f}_c\,\vec{f}_c$$

Where α_c is the dipole polarizability of core c (Ba^{2+} or He) and $\vec{f}_c$ represents the electric field at center c created by the valence electron and all other centers' cores, which is written as follow:

$$\vec{f}_c = \sum_i \frac{\vec{r_{ic}}}{r_{ic}^3}\,F_l\,(r_{ic},\ \rho_c)\ -\ \sum_{c\neq c'} \frac{\vec{R_{cc'}}}{R_{cc'}^3}\,Z_c$$

Noting that $\vec{r}_{ic}$ and $\vec{R}_{c'c}$ represent the core-electron vector and the core-core vector, respectively. Furthermore, the *l*-independent cut-off function is written as follow:

$$F_l = \left[1\ -\ \exp\left(-\frac{r_{ic}^2}{\rho_c^2}\right)\right]$$

In this framework, the electric dipole polarizabilities for the barium and helium cores are $10.3a_0^3$ and $1.383a_0^3$, respectively. The optimized cut-off parameters are 2.3674 a.u and 1.7 a.u for the barium and helium, respectively. We have used a large uncontracted basis set (Ba: 7 s/6p/5d) and (He: 4 s/3p) for both atoms. These basis sets are optimized previously in our group [23, 59] and given an excellent agreement in the computed energies compared with the NIST database [60].

2.2. Pair-wise model and optimization method

(i) The structures and stabilities of the M^{++}RG$_n$ clusters are investigated by the pair-wise model where the PES is calculated using the pair-interaction potentials: the alkaline-earth ion-rare gas interaction and the rare gas-rare gas interactions. In this context, the total potential energy of Ba^{2+}He$_n$ clusters is composed by the

Ba^{++}-He and He-He interactions and described by the following relation:

$$V(r) = \sum_{i=1}^{n} V_{Ba^{++}-He_i} + \sum_{i=1}^{n}\sum_{i<j} V_{He_i-He_j}$$

For the He-He interaction, we have used the Lennard-Jones potential [61], which is expressed by the analytical form:

$$V_{He-He}(r) = 4\,\varepsilon\left[\left(\frac{\sigma}{r}\right)^{12} - \left(\frac{\sigma}{r}\right)^{6}\right]$$

Where $2^{1/6}\sigma$ and ε represent the equilibrium bond length and the well depth of the helium-helium interaction, respectively. We use the values from [62]: $\sigma = 5.137$ bohr and $\varepsilon = 0.385\ 10^{-4}$ Hartree.

(ii) The most frequently used method, for small clusters, is the Monte Carlo simulation. The main objective of this method is to obtain the absolute minimum by exploring the PES. Indeed, it allows the system to cross potential barriers and thus to move from one potential well to another. In this calculation, we employed the Basin-Hopping method based on Monte Carlo simulation (BHMC). The adopted algorithm is effective for the global minima localization [63, 64]. This algorithm converts the potential energy surface $E(y)$, by energy minimization with respect to nuclear coordinates y, into a new form $E'(y)$ as expressed in the following: $E'(y) = \min_l\{E(y)\}$. Subsequently, this potential $E'(y)$ is explored by the Monte Carlo sampling. We can note that 10^4 cycles for each size of clusters were executed, and random displacements of all atoms were carried out.

3. Results and discussions

3.1. PES and spectroscopic parameters

The potential energy surfaces for the $^2\Sigma^+$, $^2\Pi$ and $^2\Delta$ states of the Ba$^+$He molecular ion were calculated by varying the inter-nuclear distances from 5 a.u to 200 a.u. These curves are shown in figures 2–4. For each electronic state, the spectroscopic constants are extracted and listed in table 2.

The ground and the first excited states (X$^2\Sigma^+$, 1$^2\Sigma^+$) present potential well with little depth (D$_e$ = 24.22, 13.23 cm^{-1}) located at equilibrium bond length (R$_e$ = 8.69, 8.65 a.u). Whereas, the 2$^2\Sigma^+$ state, dissociating into {Ba$^+$(6p)+He}, has a strong repulsive character. We observed a similar behavior in the $^2\Sigma^+$ state dissociating into {Ba$^+$(6p)+Xe} in [23]. A bibliographic review shows that the spectroscopic parameters for the ground state X$^2\Sigma^+$ are calculated by Buchachenko *et al* [2], McGuirk *et al* [3] and Tuttle *et al* [30]. These authors have used the RCCSD(T) and CCSD(T) method where the charged barium is described by different basis sets. An acceptable agreement is observed,
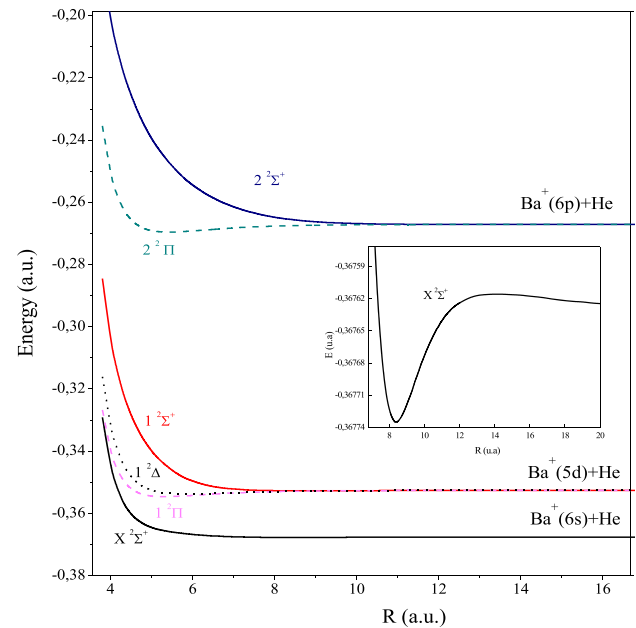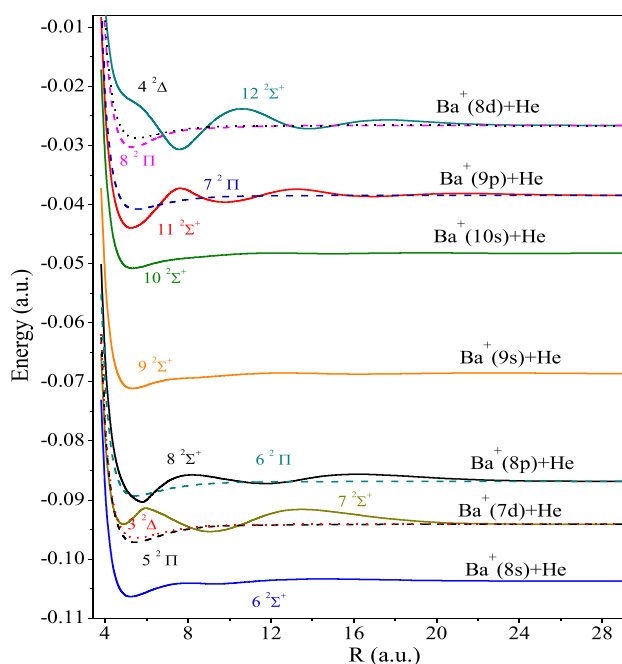

Figure 2. Potential energy surfaces (PES) of the three first limits $^2\Sigma^+$ (solid line), $^2\Pi$ (dotted line), and $^2\Delta$ (dashed line) of Ba$^+$He. The inset shows the PES for the ground state X$^2\Sigma^+$.
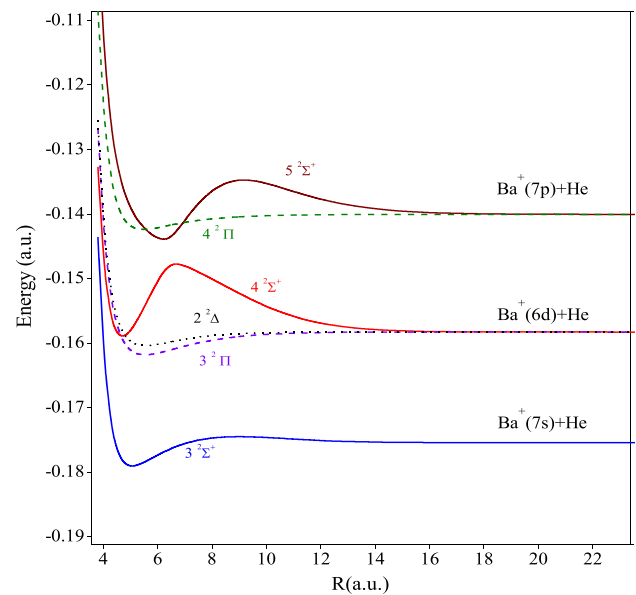
Figure 3. Potential energy surfaces of the three second limits $^2\Sigma^+$ (solid line), $^2\pi$ (dotted line), and $^2\Delta$ (dashed line) of Ba$^+$He.

especially for R$_e$, where the residual discrepancy is lower than 0.75 a.u. For dissociation energy (D$_e$), our potential is deeper than found in literature [2, 3, 30] and the average difference reaches 3.62 cm^{-1}. The comparison shows a rather good agreement for the harmonic frequency ω_e, anharmonic constant $\omega_e\chi_e$, and rotational constant B$_e$. In particular, our calculated values for D$_e$, ω_e, and $\omega_e\chi_e$ are consistent, with core ECP/BF/C5Z results obtained by Buchachenko and Viehland [2] at the RCCSD(T) level. The comparison of the anharmonic constant with the theoretical data reported by

Figure 4. Potential energy surfaces of the highest excited limites $^2\Sigma^+$ (solid line), $^2\pi$ (dotted line), and $^2\Delta$ (dashed line) of Ba$^+$He.

McGuirk *et al* [3] shows an excellent agreement with the average difference is 0.01 cm^{-1}.

Recently, Tuttle *et al* [30] studied the metal cation/rare gas (M$^+$RG) using RCCSD(T) calculations with the corresponding Dunning-type basis sets, and small-core ECPS. Several PES of the (M$^+$RG) complexes were calculated and the spectroscopic constants were derived from the ground state. The comparison of dissociation energy and the equilibrium distance is in fairly good agreement with the value reported theoretically by these authors where the differences are equal to 1.22 cm^{-1} for D_e and 0.65 a.u for R_e. In addition, Mella and Cargnoni [46] have determined, at the MRCI level of theory with Def2 pseudo-potentials and large basis sets, the PES of M$^+$He (M = Ba, Sr) for states asymptotically correlated to the lowest ^{2}P and ^{2}D limits. It is notable that our calculated parameters for the first excited state $1^2\Sigma^+$ are approximately close to those given in the literature [46] ($\Delta R_e = 5.52$ a.u. and $\Delta D_e = 9.73$ cm^{-1}). In particular, the equilibrium bond length and dissociation energies for the $1^2\Pi$ and $1^2\Delta$ states are in favorable agreement with the present results where the differences are 0.19 a.u for R_e and 15 cm^{-1} for D_e. In contrast, we note a great difference in the second excited state $2^2\Sigma^+$ that we find a repulsive character using the ECP-CPP and full valence CI theory, while Mella and Cargnoni [46] have shown an attractive potential with a small well (~9 cm^{-1}). This difference can be explained by the diversity in the basis set used and the different techniques of calculation. One can notice that we need experimental results on this molecule.

From inspection of figures 3 and 4, the higher excited states have an interesting behavior imprinted by the existence of avoided crossings which well explained the interplay between repulsive and attractive effects. At these positions,

the energy difference between the involved states is very small compared to other positions. For example, the small difference is detected for $(4\text{–}5)^2\Sigma^+$ ($\Delta E < 400$ cm^{-1}) and $(7\text{–}8)^2\Sigma^+$ ($\Delta E < 160$ cm^{-1}) which could lead to non-adiabatic transitions. Accordingly, several states have a double-well structure, where the outer well is shallow and placed at a larger distance. For instance, the second well depth for the sixth state is 102 cm^{-1} at the equilibrium bond length $R_e = 9.3$ a.u. We can explain this structure by the forte penetration of the helium atom in the electronic cloud through the Rydberg electron in these states. That leads to an inner well affected to the equilibrium between repulsive and attractive forces. Furthermore, we observe the appearance of barrier structure or humps, especially in the $^2\Sigma^+$ electronic states correlated to 6d and 7p limits. This behavior can be explained by the repulsion interaction between the Rydberg electron and the helium atom. We note that the $4^2\Sigma^+$ {Ba$^+$(6d)+He} state posses the highest barrier structure where their energy is around 1800 cm^{-1} at the internuclear separation $R_{max} = 6.67$ a.u. While, In the Ba$^+$Xe system [23], the highest barrier is found for the {Ba$^+$(7p) + Xe} limit. This difference can be related to the influence of the noble gas size on the repulsive character of the electron-helium interaction. Concerning the $5^2\Sigma^+$ electronic state, the energy of humps is $E_b = 900$ cm^{-1} located at $R_{max} = 9.1$ a.u. The comparison of $4^2\Sigma^+$ and $5^2\Sigma^+$ states shows that the energies of humps decrease when the barrier position increase. This is due to the repulsive effects which become weaker for the highest excited states.

The PES of $^2\Pi$ and $^2\Delta$ electronic states present a regular shape with simple potential well. It is worthy to note that the potential wells for the first $^2\Pi$ and $^2\Delta$ states are far deeper than those of $^2\Sigma^+$ states. This is not surprising since, the orbitals of Π and Δ symmetries, perpendicular to the molecular axis, are implicated and the repulsive electron-helium interaction is consequently much weaker. Accordingly, the $^2\Pi$ states correlated to 5d, 6d, 7d, and 8d limit have deeper potential well than the doublet Δ states, where their depths change significantly from one limit to the other. This comportment is appeared previously in Ba$^+$Xe [23] and Mg$^+$Ar [65] van der Waals complexes.

Besides, we have investigated the impact of the second valence electron on the PES for the neutral system BaHe. The computed curves of $(9)^{1,3}\Sigma^+$, $(8)^{1,3}\Pi$ and $(4)^{1,3}\Delta$ states are plotted in figure 5. The study of van der Waals complex of barium atom interacted with the light noble gas helium shows a repulsive character in PES for the first excited states of sigma symmetries except the $3^1\Sigma^+$ and $4^{1,3}\Sigma^+$ states. These results are consistent with those calculated by Czuchaj *et al* [26]. We detect an avoided crossing between $3^1\Sigma^+$ and $4^1\Sigma^+$ at $R_{AC} = 8.13$ a.u with a minimal energy difference equal to 61 cm^{-1}. At this position, the non-adiabatic transitions could be possible. We can see from figure 5 that the $4^1\Sigma^+$ and $4^3\Sigma^+$ states having potential-barrier structures with the energy of humps are 557 cm^{-1} and 438 cm^{-1} at R = 5.98 and a.u R = 7.78 a.u, respectively. Concerning the Π symmetry, all curves present regular behaviors with simple potential well. Their depths are shallow for the low-lying states and become

Table 2. Spectroscopic constant for the $^2\Sigma^+$, $^2\Pi$, and $^2\Delta$ states of Ba$^+$He molecular ion. (Vertical transition energy T$_e$).

States	R_e(a.u.)	D_e (cm^{-1})	T_e (cm^{-1})	ω_e (cm^{-1})	$\omega_e\chi_e$ (cm^{-1})	B_e (cm^{-1})
X $^2\Sigma^+$	8.69	24.22	0	17.2	3.40	0.205
	[9.44][a]	[20.60][a]		[15.9][a]	[3.26][a]	
	{9.29}[a]	{22.6}[a]		{17.2}[a]	{3.99 }[a]	
	9.35[b]	21.8[b]		16.7[b]	3.39[b]	0.183[b]
	9.28[c]	23[c]		19.6[c]	4.65[c]	0.185[c]
1$^2\Sigma^+$	8.65	13.23	3343	4.32	0.89	0.206
	14.17[d]	3.50[d]				
2$^2\Sigma^+$	—	—	22475	—	—	—
	10.85[d]	9.30[d]				
3$^2\Sigma^+$	5.06	790.05	42496	245	13.85	0.606
4$^2\Sigma^+$	4.69	137.06	47558	422	10.32	0.703
5$^2\Sigma^+$	6.21	845.82	51198	252	5.43	0.401
6$^2\Sigma^+$	5.24	608.43	57925	184	15.60	0.563
2nd min	9.30	102.27				
7$^2\Sigma^+$	4.88	506.53	59856	87	1.98	0.187
2nd min	9.08	753.29				
8$^2\Sigma^+$	5.79	969.72	61972	156	7.36	0.463
2nd min	11.77	278.82				
9$^2\Sigma^+$	5.32	564.43	65641	138	9.46	0.546
10$^2\Sigma^+$	5.33	559.06	70050	145	10.27	0.544
11$^2\Sigma^+$	5.26	1210.93	72252	224	9.78	0.559
2nd min	9.76	246.59				
3rd min	16.79	78.18				
12$^2\Sigma^+$	7.59	997.88	74691	286	22.02	0.268
2nd min	13.78	233.12				
1$^2\Pi$	5.29	448.97	3343	147	12.24	0.553
	5.48[d]	486.60[d]				
2$^2\Pi$	5.41	531.33	21817	154	11.20	0.528
	5.40[d]	388.90[d]				
3$^2\Pi$	5.53	771.67	45707	154	6.87	0.508
4$^2\Pi$	5.47	513.19	49935	133	8.88	0.517
5$^2\Pi$	5.45	675.94	60035	155	9.09	0.521
6$^2\Pi$	5.47	535.27	61533	134	8.55	0.517
7$^2\Pi$	5.51	509.22	72255	133	8.77	0.509
8$^2\Pi$	5.31	812.18	74866	184	10.82	0.549
1$^2\Delta$	6.03	196.42	3343	95	11.93	0.426
	5.84[d]	211.90[d]				
2$^2\Delta$	5.49	441.37	46157	131	9.78	0.513
3$^2\Delta$	5.48	504.73	60041	137	9.53	0.517
4$^2\Delta$	5.51	447.73	75069	130	9.54	0.509

[a] (Theoretical values in square brackets are the nonsmall core ECP/CTZ results and values in braces are the nonsmall core ECP/BF/C5Z results from [2]);
[b] (Theoretical values calculated at the RCCSD(T) method from [3]);
[c] (Theoretical values calculated at the RCCSD(T) method with the corresponding Dunning-type basis sets, and small-core ECPS from [30]);
[d] (Theoretical values calculated at the MRCI level with Def2 pseudo-potentials and extended basis sets from [46]).

significant for the superior excited states like $3^{1,3}\Pi$ and $4^{1,3}\Pi$. We observe that the triplet states are much deeper than the singlet ones. For instance, the $(2, 4)^3\Pi$ states are attractive and the $(2, 4)^1\Pi$ states are repulsive. We note the same interpretation for $2^1\Delta$ and $2^3\Delta$ states where the triplet has an attractive potential well (D$_e$ = 280 cm^{-1}), while the singlet has a repulsive one. This means that the repulsive interaction between valence electrons and helium element for triplet symmetries is inferior to singlet one.

On the first hand, we compare the well depths of the ground state for Ba^{++}He, Ba$^+$He, and BaHe systems in order to highlight the strong repulsion of the neutral system compared to ionic ones. Figure 6 shows an important decrease in the potential well depth going from Ba^{++}He to BaHe. In fact, the well depth is about 558 cm^{-1} for Ba^{++}He, then decreases to 24.22 cm^{-1} for Ba$^+$He until becomes repulsive for the neutral molecule BaHe. The variation in well depth is explained by the strong repulsion for the electron helium interaction, particularly in Σ^+ symmetry, when orbital along the molecular axis is involved.

On the other hand, we report, in table 3, a comparative study of the AE$^+$-He and Ba$^+$-RG [3, 23, 24, 38, 39, 41, 66]
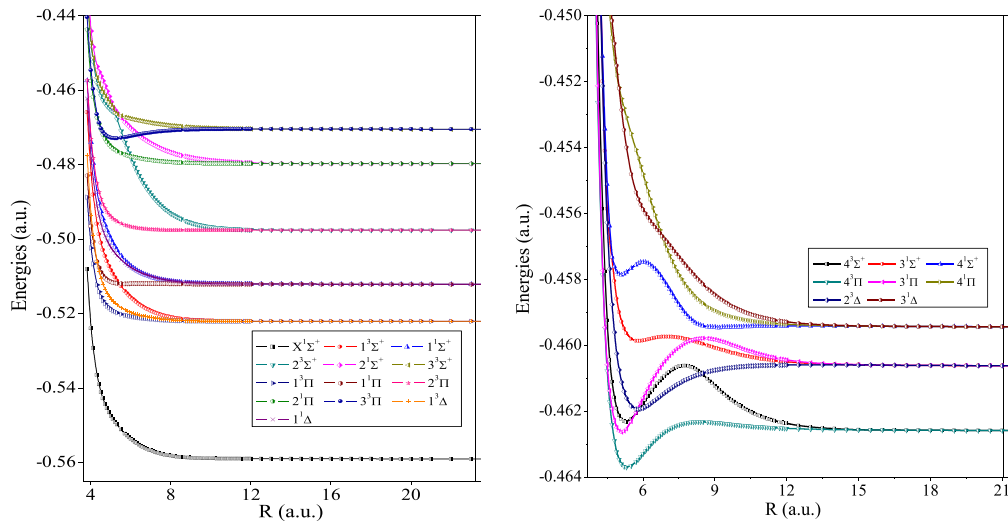
Figure 5. Potential energy surfaces for the $^{1,3}\Sigma^+$, $^{1,3}\Pi$, and $^{1,3}\Delta$ of BaHe van der Waals system.
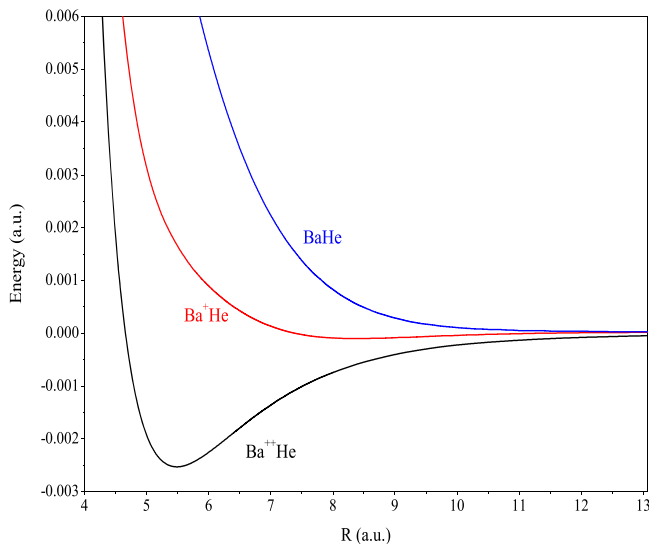
Figure 6. Comparison between potential energy surfaces for Ba^{++}He, Ba$^+$He, and BaHe van der Waals systems.

Table 3. Comparison of spectroscopic data for AE$^+$He and Ba$^+$RG systems.

Systems	R_e (Å)	D_e (cm^{-1})	ω_e (cm^{-1})
Be$^+$He	2.96[a]	124[a]	73[a]
Mg$^+$He	3.46[b]	54[b]	48.42[b]
Ca$^+$He	3.88[c]	51[c]	45[c]
Sr$^+$He	4.55[d]	29[d]	21[d]
Ba$^+$He	4.60	24.22	17.2
Ba$^+$Ne	4.29[e]	72[e]	15[e]
Ba$^+$Ar	3.36[f]	850 ± 150[f]	61[f]
Ba$^+$Kr	3.59[g]	1243[g]	50[g]
Ba$^+$Xe	3.77[h]	1971[h]	54[h]

[a] [41];
[b] [39];
[c] [38];
[d] [12];
[e] [3];
[f] [67];
[g] [24];
[h] [23].

to explain the effect of noble gas size on the spectroscopic properties of Ba$^+$-complexes as well as the influence of the alkaline-earth size on the He-complexes.

We note that for the AE$^+$-He complexes, the equilibrium bond length values generally show an overall increase with increasing atomic number of the alkaline-earth cation. While the dissociation energy and harmonic frequency values exhibit decrease significantly with increasing the alkaline-earth cation size. These variations are explained by the notable growth of the repulsive interaction between helium and alkaline-earth cation from beryllium to barium, which reduces the well depth and shift the equilibrium to the large distances.

In addition, the influence of the noble gas size on the properties of Ba$^+$-complexes is clearly observed in table 3. We can note that the increase values in well depth from Ba$^+$He to Ba$^+$Xe are related to the significant increase in the rare gas polarizabilities (from $\alpha_{He} = 1.383\ a_0^3$ to $\alpha_{Xe} = 7.295$

a_0^3). The increase in ω_e values is a logical result of the increase in D_e values when the rare gas size varies from helium to xenon. The atomic number and size of the rare gas generate a remarkable decrease in equilibrium bond length values.

3.2. Vibrational and electric dipole properties

This section is focused on the vibrational and electric dipole properties of the Ba$^+$He van der Waals system. The vibrational levels energies have been calculated for $^2\Sigma^+$, $^2\Pi$, and $^2\Delta$ adiabatic states by solving the radial Schrodinger equation. The vibrational levels numbers (N_v) are listed in table 4. The ground and first excited states have one vibrational level ($N_v = 1$). This result is obviously related to the shallowness of their potential wells ($D_e = 24.22$ and 13.23 cm^{-1}). It is worthy to note that the N_v increase when

Table 4. Vibrationnal levels number (N_v) for $^2\Sigma^+$, $^2\Pi$ and $^2\Delta$ states of the Ba$^+$He system.

States	N_v	States	N_v	States	N_v
X $^2\Sigma^+$	1	9 $^2\Sigma^+$	10	6 $^2\Pi$	9
1 $^2\Sigma^+$	1	10 $^2\Sigma^+$	9	7 $^2\Pi$	8
2 $^2\Sigma^+$	0	11 $^2\Sigma^+$	13	8 $^2\Pi$	10
3 $^2\Sigma^+$	6	12 $^2\Sigma^+$	8	1 $^2\Delta$	3
4 $^2\Sigma^+$	7	1 $^2\Pi$	5	2 $^2\Delta$	6
5 $^2\Sigma^+$	10	2 $^2\Pi$	6	3 $^2\Delta$	7
6 $^2\Sigma^+$	7	3 $^2\Pi$	10	4 $^2\Delta$	7
7 $^2\Sigma^+$	13	4 $^2\Pi$	8		
8 $^2\Sigma^+$	13	5 $^2\Pi$	10		

Figure 7. Vibrational level spacings (E_{v+1}-E_v): (a) for $^2\Sigma^+$ states and (b) for $^2\Pi$ and $^2\Delta$ states.

the potential well of the associated states becomes deeper. For instance, we get 10 and 13 levels, respectively, for $5^2\Sigma^+$ and $7^2\Sigma^+$ excited states. As usual, the electronic states without any vibrational levels such as $2^2\Sigma^+$ are repulsive as shown previously in PES.

In figure 7, we have plotted the vibrational level spacing (E_{v+1}-E_v) according to the vibrational levels' number v for several states of the symmetries $^2\Sigma^+$, $^2\Pi$ and $^2\Delta$. While, in table 5, we have reported the vibrational levels spacing for the remaining states. The inspection of this figure shows that the vibrational level spacing decreases as the vibrational levels' number v increases and finally vanishes. Also, linear behaviors are observed for low vibrational level v reflecting a Morse-like anharmonicity. The spacings for 6, 7 and $8^2\Sigma^+$ excited states present an abrupt variation manifested by an accidental quasi-degeneracy that emerged twice, signifying the appearance of a second well. For instance, in the case of $7^2\Sigma^+$ state, a linear behavior is observed for the first levels which imprinted by the usual anharmonicity of the inner well. Then accidental quasi-degeneracy occurs at $v = 5$ and $v = 10$ when the outer well appears at $R_e = 9.08$ a.u. Furthermore, a specific behavior is detected for the higher excited state which confirms their shape in the PES. Clearly, for the $11^2\Sigma^+$, the spaces show a linear behavior up to $v = 4$ associated with an anharmonic potential. An abrupt change is registered several times at $v = 5$, 8 and 12, which is corresponding to the accidental degeneracy and the appearance of multiple minima. The examination of table 4 shows that $X^2\Sigma^+$ and $1^2\Sigma^+$ having only one vibrational level, which reflects the shallowness of the width of the well of potential ($D_e = 24.22$, 13.23 cm^{-1}). We detect numerous vibrational levels trap in 7, 8 and $11^2\Sigma^+$ states. These latter shed light on the importance of the width of the well of potential at the level of the dissociated limit. Concerning the $^2\Pi$ and $^2\Delta$ symmetries, their vibrational level spacing presents an unusual variation which confirms the behavior in PES. The spacings curves progressively decrease according to v and become minimal towards the asymptotic limit.

The electric dipole moment for van der Waals complexes provides interesting information to experimental studies such as, to obtain the transmission spectrum and the rotationally resolved absorption spectrum [67–69] in alkaline-earth-rare gas systems. For this aim, we have calculated the Permanent
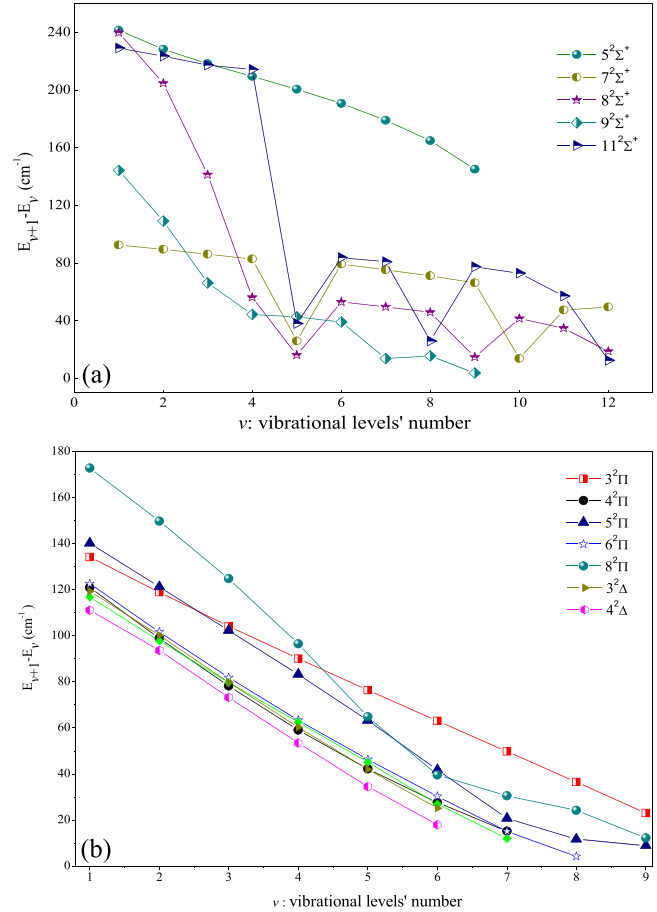
Dipole Moment (PDM) for the ground and excited $^2\Sigma^+$ states of Ba$^+$He. These curves are drawn in figure 8 as a function of the internuclear distance R. The inspection of this figure shows that the important variations are detected only at short distances (R < 20 a.u) where changes occurred in their electronic wave-function. At large internuclear distances, all PDM functions tend to zero; except for $6^2\Sigma^+$, $8^2\Sigma^+$ and $11^2\Sigma^+$ states, they tend to constant. Additionally, the PDM functions for the low-lying states (X-3) $^2\Sigma^+$ have regular behavior with single extrema reflecting the regular form of the anharmonic potential well. The ground state $X^2\Sigma^+$ has a small dipole moment value ($\mu = 0.26$ a.u) at R around 5 a.u. For $3^2\Sigma^+$ state, its variation in PDM function shows a maximum of 1.47 a.u at the interatomic distance of 5.43 a.u. While irregular variations are obtained in the higher $^2\Sigma^+$ states due to the barrier structure and the existence of avoided crossings in their PES. As illustrated in figure 8, the PDM function for $5^2\Sigma^+$ state presents two different extrema located at short distances $R_1 = 5.85$ a.u ($\mu_1 = 0.124$ a.u) and $R_2 = 8.17$ a.u ($\mu_2 = 0.11$ a.u) where the first and second positions are related to the equilibrium and the hump positions in their potential curve, respectively. More significantly, the highest PDM value for Ba$^+$He is localized in the $6^2\Sigma^+$ state dissociating into 8 s limit. While significant variations in PDM curves are present for states correlating to 5d and 6p
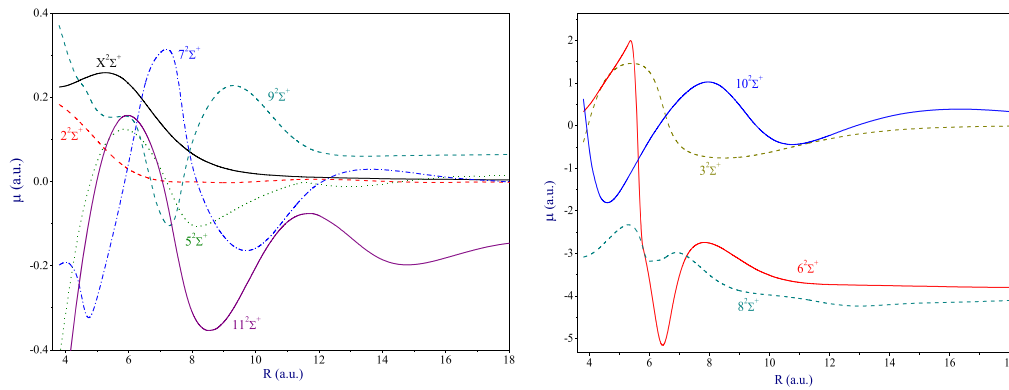
Figure 8. PDM curves for the ground and excited $^2\Sigma^+$ states of Ba$^+$He.

Table 5. Vibrational level spacings ($E_{v+1} - E_v$) for selected states of the Ba$^+$He system (in cm^{-1}).

N_v	$3\ ^2\Sigma^+$	$4\ ^2\Sigma^+$	$6\ ^2\Sigma^+$	$10\ ^2\Sigma^+$	$12\ ^2\Sigma^+$	$1\ ^2\Pi$	$2\ ^2\Pi$	$7\ ^2\Pi$	$1\ ^2\Delta$	$2\ ^2\Delta$
1	217.86	395.23	161.74	135.72	224.48	123.00	132.59	116.89	71.85	110.99
2	189.61	379.41	134.23	103.14	202.74	97.70	109.45	97.81	47.98	93.46
3	162.21	363.10	98.56	73.10	185.11	73.25	86.84	79.80		73.01
4	135.06	345.41	14.18	55.08	75.55	49.52	64.71	62.55		53.02
5	106.34	324.12	36.52	48.17	79.82		42.94	45.17		33.77
6		284.18	31.11	41.97	12.57			26.90		
7				19.18	74.84			11.95		
8				10.98						

limits for Ba$^+$Kr [24] and Ba$^+$Xe [23] respectively. This proves the influence of the size of rare gas atoms in the Rydberg state in the electric dipole moment functions.
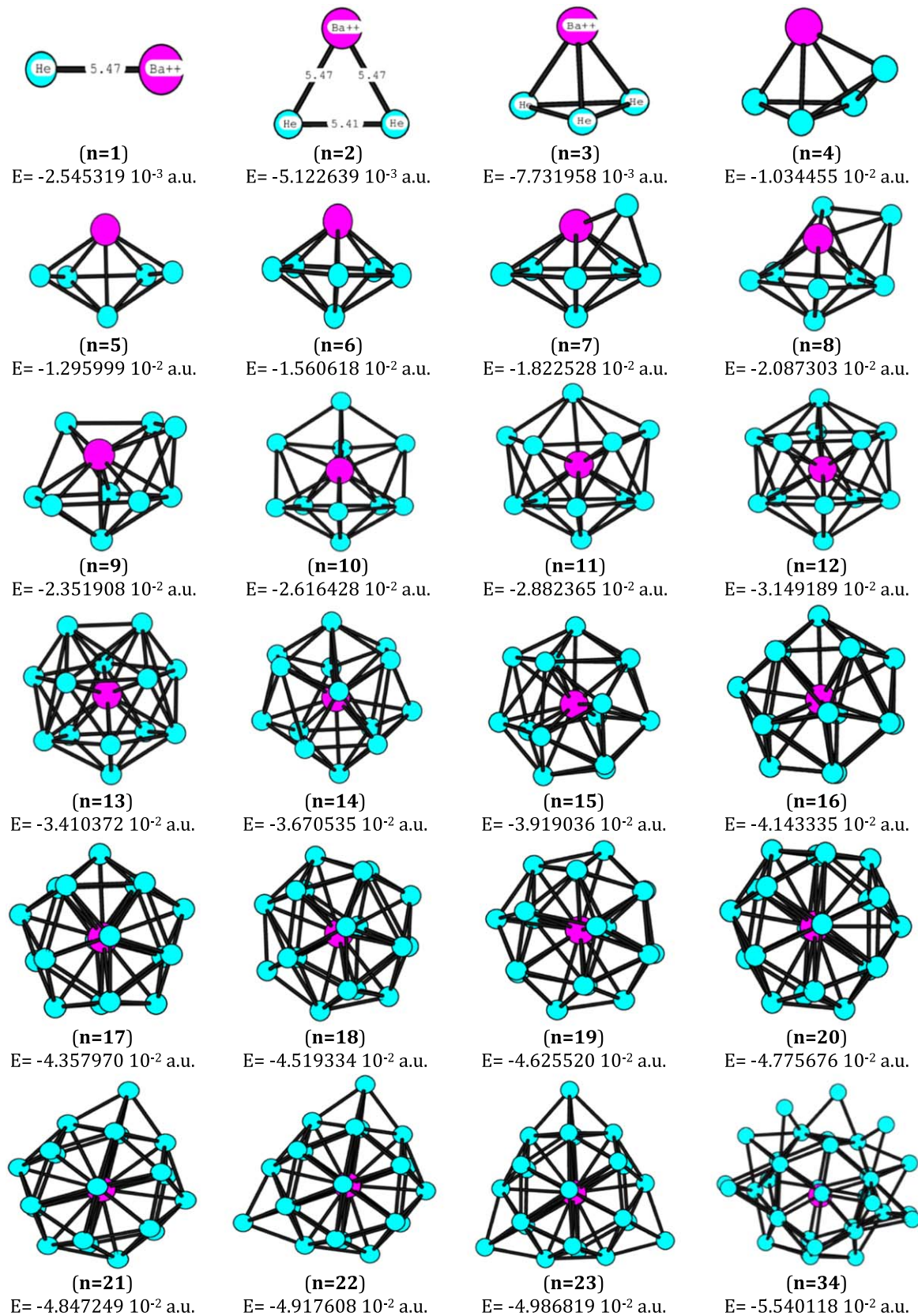
3.3. The stable geometry for Ba^{++}He$_n$ clusters

In this section, we will discuss the geometries of the Ba^{++}He$_n$ complexes. To our best knowledge, the Ba^{++}He$_n$ clusters calculated by the Monte Carlo simulation are original and never published previously. Several subsequent works have been focused on alkali doped helium clusters. They have suggested that the size of snowballs depends on the electronic structure of the impurity. For instance, the experimental results for the Na$^+$He$_n$ [70] found that the snowball is complete at n = 9. Coccia and co-workers [71] showed that for Li$^+$, Na$^+$ and K$^+$ immersed in helium solvent, the first solvation shell completion being reached at sizes 10, 12, and 15, respectively. For Mg^{2+}He$_n$, it was found the closure of the first solvation shell at size 9 [47].
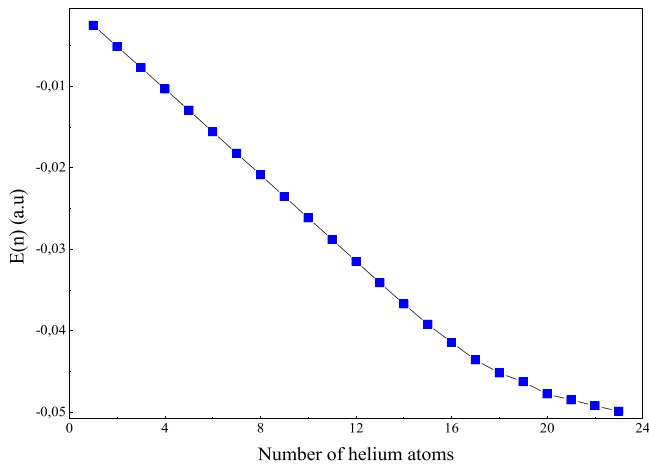
The structures and relative stabilities of the Ba^{++}He$_n$ mixed clusters are investigated by the pairwise model where the PES is calculated using the pair-additive potentials. The PES of Ba^{++}He$_n$ is described by the Ba^{++}He potential and He-He interaction by means of Tang-Toennies and Lennard-Jones potentials model, respectively. Then this PES is explored by the Monte Carlo basin-hopping method, to carry out the geometries of Ba^{++}He$_n$ clusters. It is worthily noticeable that the pairwise model deals with 2-body interactions Ba^{++}-He and He–He where the charge remains essentially localized on the impurity. Hence, the interactions between the dipole moments induced by the barium cation on helium atoms

(induced dipole-induced dipole) and the effect of the electric field created on each polarizable site by the induced dipoles themselves (charge-induced dipole) are not considered, in view of the low polarizability of the helium atom. Actually, in the case of the helium solvent, the role of more accurate interactions beyond two-body terms has mostly been addressed at the *ab initio* level [43, 44, 47] or with explicit three-body contributions between induced dipoles [72]. It has been shown that the inclusion of the leading terms of such many-body forces does not alter substantially the structure of the clusters [72–74], which is not surprising in light of the weak polarizability of the helium atom. However, this is not the case for the heavier rare gas where the many-body forces could play the main role [75, 76]. Indeed earlier work [77] has shown that already in Ca^{2+}Xe$_n$ clusters many-body forces may induce significant changes in the stable structures, especially at small sizes, where the induced dipole-induced dipole contribution affect the geometries in a repulsive manner.

The lowest-energy structures of Ba^{++}He$_n$ clusters as a function of size are shown in figure 9. The Ba^{++}He has a linear structure (D_∞ symmetry) with minimum energy equal to 558 cm^{-1} and equilibrium bond length equal to 5.47 a$_0$. Triangular structure with Ba^{++} cation occupying the summit position is obtained for Ba^{++}He$_2$ cluster (C_{2V} symmetry), where the Ba^{++}-He and He-He equilibrium bonds are respectively, 5.47 a$_0$ and 5.41 a$_0$. The most stable structure for the Ba^{++}He$_3$ cluster is trigonal pyramid geometry with C_{3v} symmetry. For n = 4, the corresponding structure has C_{2v} symmetry where two triangular pyramids share a common face. The Ba^{++}He$_5$ geometry is described by a C_s symmetry.

(n=1)
E= -2.545319 10⁻³ a.u.

(n=2)
E= -5.122639 10⁻³ a.u.

(n=3)
E= -7.731958 10⁻³ a.u.

(n=4)
E= -1.034455 10⁻² a.u.

(n=5)
E= -1.295999 10⁻² a.u.

(n=6)
E= -1.560618 10⁻² a.u.

(n=7)
E= -1.822528 10⁻² a.u.

(n=8)
E= -2.087303 10⁻² a.u.

(n=9)
E= -2.351908 10⁻² a.u.

(n=10)
E= -2.616428 10⁻² a.u.

(n=11)
E= -2.882365 10⁻² a.u.

(n=12)
E= -3.149189 10⁻² a.u.

(n=13)
E= -3.410372 10⁻² a.u.

(n=14)
E= -3.670535 10⁻² a.u.

(n=15)
E= -3.919036 10⁻² a.u.

(n=16)
E= -4.143335 10⁻² a.u.

(n=17)
E= -4.357970 10⁻² a.u.

(n=18)
E= -4.519334 10⁻² a.u.

(n=19)
E= -4.625520 10⁻² a.u.

(n=20)
E= -4.775676 10⁻² a.u.

(n=21)
E= -4.847249 10⁻² a.u.

(n=22)
E= -4.917608 10⁻² a.u.

(n=23)
E= -4.986819 10⁻² a.u.

(n=34)
E= -5.540118 10⁻² a.u.

Figure 9. The lowest-energy structures for $Ba^{++}He_n$ clusters (n = 1–23 and 34).

Figure 10. Binding energies as a function of size for stable structures of $Ba^{++}He_n$ clusters.

Figure 11. Second-energy difference as a function of cluster size for $Ba^{++}He_n$ clusters.

An additional helium atom leads to a more stable structure described by a regular pentagonal bipyramid with C_{5v} symmetry. By adding more He atoms, we generate a series of minima with the extra atoms on the same side as barium, thus closing the cation in the interior of the cluster. The onset of the icosahedral structure is indicated for n = 10, which is completed at n = 12. Thus, the regular icosahedron is formed with I_h high symmetry. To confirm the stable structure of the $Ba^{++}He_{12}$ cluster, we use a simple hard sphere packing model reported by Lüder *et al* [78]. Indeed, this model predicts that if the distance ratio d^* obey the following condition: $0.8226 \leqslant d^* = \frac{d_{Ba^{++}-He}}{d_{He-He}} \leqslant 0.951$, then the most favorable structure is icosahedral. In our case, the distance between the central cation and the helium atom is $d_{Ba^{++}-He} = 5.457$ a.u. and the distance between two helium atoms is $d_{He-He} = 5.96$ a.u. We obtain $d^* = 0.9156$, which confirms the icosahedral symmetry for $Ba^{++}He_{12}$.

Beyond n = 12, we remark that the extra helium atoms are not deposed on the triangular faces of the icosahedron in contrast with pure van der Waals clusters which are dominated by polyicosahedral growth. The heterogeneity in the Ba^{++}-He and He–He interactions make the growth more isotropic around the cation, a feature that can also be seen as a manifestation of geometric frustration. Indeed, doping helium clusters by positive ions induces local enhancement of the helium density by electrostriction. A solid-like structure produces around Ba^{++}; such a structure is called a 'snowball'. At n = 20, the twenty helium atoms complete the first solvation shell in a rigid arrangement around the cation. Afterward this size, the added helium atoms are localized on the faces of the $Ba^{++}He_{20}$ and the building of the second solvation shell begins. At larger sizes, the He-He bonds predominate and increasingly inclined to vibrational delocalization.

The binding energies of the $Ba^{++}He_n$ clusters are represented in figure 10 as a function of their size. This curve shows clearly two regimes n < 19 and n > 20 with different slopes. The first regime is predominated by the Ba^{++}–He bounds, the helium atoms are covered the cation until we reach the first solvation shell with twenty–helium snowball.
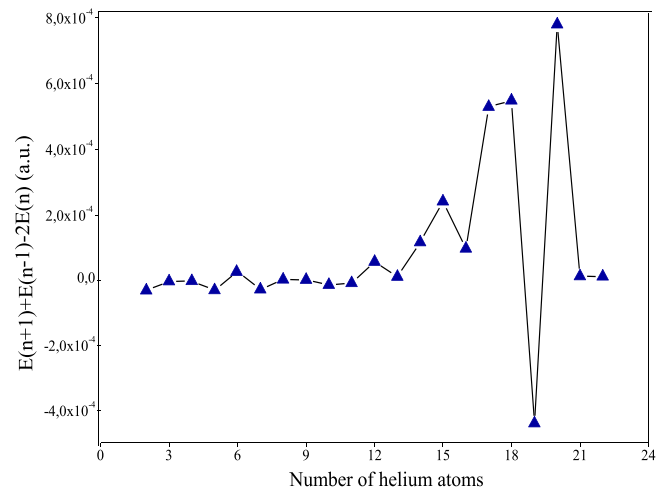
The binding energies curve shows a clear accident at n = 19; the $Ba^{++}He_{19}$ cluster being rather unstable. For the upper sizes n > 20, the growth mechanism is associated with the predominance of the attractive interactions between helium atoms. In fact, this regime presents a little size effect.

In order to examine the relative stability of diverse cluster sizes for $Ba^{++}He_n$, we have calculated the second-energy difference {E(n + 1) + E(n − 1) – 2E(n)}, plotted in figure 11. The second-energy difference is especially suitable to scrutinize the different regimes discussed above. A small size effect is observed at n < 6, where the helium atoms start to cover Ba^{++} on the side. Thereafter, the helium atoms cover the impurity more isotropically in the size range of $6 \leqslant n \leqslant 12$ where Ba^{++} is appeared totally solvated at n = 12 with the formation of a regular icosahedron (I_h). The second-energy difference curve shows a drop in intensity at n = 11 and n = 13 which indicates the instability of these clusters. Then, in the size range of $14 \leqslant n \leqslant 20$, the variation is more regular and more isotropic where the first solvation shell is being formed. We notice peaks at n = 15, 18 and 20 as magic numbers which are related to the high stability of the corresponding geometries. The most intense peak is marked at n = 20 which is associated with the completion of the first solvation shell with the formation of twenty-helium snowball. It is worthy to note that the curve shows a drop in intensity at n = 19 and n = 21, which is related to the destruction of the high stability of the twenty-helium snowball. Besides, a small size effect is marked for the upper sizes n > 20 where the growth mechanism is predominated by the He-He bonds.

4. Conclusion

In the present work, the electronic properties of $Ba^{0,+,2+}He$ van der Waals systems have been investigated. The $Ba^{++}He$ core-core interaction potential has been performed by the CCSD(T) theory. A comparison between our potential and the available studies has shown a good agreement, which validates its precision and its use in the modeling of the $Ba^{0,}He$ van der Waals

systems. In addition, one and two-electron computations along with CPP approach, for the ground and several electronic excited states, of Ba^+He and $BaHe$ systems have been realized. Owing to single and double valence electron systems large basis sets for both elements (Ba and He) were used. The obtained spectroscopic parameters were in agreement with the few available results mainly for the ground state $X^2\Sigma^+$ of Ba^+He, which provides assurance in our used theoretical approach. Several states appear with a double-well structure, which may be related to the high penetration of helium atom the electronic cloud through the Rydberg electron in these states. That gives rise to an inner well assigned to the equilibrium between attractive and repulsive forces. Unlike the ionic van der Waals system, where most states of the $BaHe$ are practically repulsive and some of them have humps such as $4^{1,3}\Sigma^+$ and $3^1\Pi$ states. The comparison between PES for $BaHe$, Ba^+He and $Ba^{2+}He$ van der Waals complexes, shows that the repulsive character of the electrons-He interaction is dominated especially in $\sum$ symmetries.

In the current work, the structures and relative stabilities of $Ba^{++}He_n$ ($n < 24$, $n = 34$) clusters have been investigated using the pair-wise model. We found that the cation is well localized at the center of the cluster with the formation of a 'snowball' of well-defined shell of localized helium atoms around Ba^{++}. Such effect (snowballing) is due to the electrostriction effect which consists in the increase of the local He density in the proximity of the cation.

The first solvation shell consists of 20 helium atoms and the additional atoms are localized on the faces of the $Ba^{++}He_{20}$ cluster. The relative stability of $Ba^{++}He_n$ clusters was examined by computing the binding energy per number of helium atoms and the second order difference in energy. Accordingly, magic numbers were found at $n = 6, 12, 15, 17, 18, 20$ which indicates the stable character of these clusters. The most intense peak is marked at $n = 20$ which is associated with the completion of the first solvation shell.

Most of these results are original and have not yet been presented in previous work. This contribution could be extended by taking into account the many-body effects on the structures and stabilities of $Ba^{++}He_n$ clusters. We prospect that the accurate data produced for the ground and for the excited states of the Ba^+He will be used to study the stability of Ba^+He_n clusters and to investigate the broadening effect of the barium ion spectrum by collision with the helium gas. We hope that our results will open up possibilities for testing the modeling of super-fluid and solid quantum matrix-isolated barium atoms.

ORCID iDs

Mtiri Safa ⓘ https://orcid.org/0000-0002-0012-5087

References

[1] Batulin R, Moroshkin P, Tayurskii D A and Kono K 2018 Spectroscopy of Ba^+ ions in liquid ^4He AIP Adv. **8** 15328

[2] Buchachenko A A and Viehland L A 2018 Interaction potentials and transport properties of Ba, Ba^+, and Ba^{2+} in rare gases from He to Xe J. Chem. Phys. **148** 154304

[3] McGuirk M F, Viehland L A, Lee E P, Breckenridge W H, Withers C D, Gardner A M, Plowright R J and Wright T G 2009 Theoretical study of Ba^{n+}–RG (RG = rare gas) complexes and transport of Ba^{n+} through RG (n = 1, 2; RG = He–Rn) J. Chem. Phys. **130** 194305

[4] Masson A, Heitz M-C, Mestdagh J-M, Gaveau M-A, Poisson L and Spiegelman F 2014 Coupled electronic and structural relaxation pathways in the postexcitation dynamics of Rydberg states of $BaAr_N$ Clusters Phys. Rev. Lett. **113** 123005

[5] Kanorsky S I, Arndt M, Dziewior R, Weis A and Hänsch T W 1994 Pressure shift and broadening of the resonance line of barium atoms in liquid helium Phys. Rev. B **50** 6296

[6] Kanorsky S I, Arndt M, Dziewior R, Weis A and Hänsch T W 1994 Optical spectroscopy of atoms trapped in solid helium Phys. Rev. B **49** 3645

[7] Masson A, Poisson L, Gaveau M-A, Soep B, Mestdagh J-M, Mazet V and Spiegelman F 2010 Dynamics of highly excited barium atoms deposited on large argon clusters. I. General trends J. Chem. Phys. **133** 054307

[8] Viehland L A, Johnsen R, Gray B R and Wright T G 2016 Transport coefficients of He^+ ions in helium J. Chem. Phys. **144** 074306

[9] Viehland L A, Lozeille J, Soldán P, Lee E P and Wright T G 2004 Spectroscopy of K^+Rg and transport coefficients of K^+ in Rg (Rg = He–Rn) J. Chem. Phys. **121** 341–51

[10] Breckenridge W H, Ayles V L and Wright T G 2007 Analysis of the bonding in alkali-cation/Rg complexes (Rg = He–Xe) using a simple model potential Chem. Phys. **333** 77–84

[11] Hickling H L, Viehland L A, Shepherd D T, Soldàn P, Lee E P and Wright T G 2004 Spectroscopy of M^+Rg and transport coefficients of M^+ in Rg (M = Rb–Fr; Rg = He–Rn) Phys. Chem. Chem. Phys. **6** 4233–9

[12] Gardner A M, Withers C D, Wright T G, Kaplan K I, Chapman C Y, Viehland L A, Lee E P and Breckenridge W H 2010 Theoretical study of the bonding in M^{n+}-RG complexes and the transport of M^{n+} through rare gas (M = Ca, Sr, and Ra; n = 1 and 2; and RG = He–Rn) J. Chem. Phys. **132** 054302

[13] Gardner A M, Withers C D, Graneek J B, Wright T G, Viehland L A and Breckenridge W H 2010 Theoretical Study of M^+–RG and M^{2+}–RG Complexes and Transport of M^+ through RG (M = Be and Mg, RG = He−Rn) J. Phys. Chem. A **114** 7631–41

[14] Lebedev V, Moroshkin P and Weis A 2011 Spectroscopy of barium atoms in liquid and solid helium matrices Phys. Rev. A **84** 022502

[15] Harima H, Tachibana K and Urano Y 1982 Empirical interatomic potentials for Ba-rare-gas systems deduced from an absorption measurement J. Phys. B: At. Mol. Phys. **15** 3679

[16] Koyanagi G K and Bohme D K 2010 Strong closed-shell interactions: observed formation of $BaRg^{2+}$ molecules in the gas phase at room temperature J. Phys. Chem. Lett. **1** 41–4

[17] Dressler R A, Meyer H, Langford A O, Bierbaum V M and Leone S R 1987 Direct observation of Ba^+ velocity distributions in a drift tube using single-frequency laser-induced fluorescence J. Chem. Phys. **87** 5578–9

[18] Dressler R A, Beijers J P M, Meyer H, Penn S M, Bierbaum V M and Leone S R 1988 Laser probing of ion velocity distributions in drift fields: parallel and perpendicular temperatures and mobility for Ba^+ in He J. Chem. Phys. **89** 4707–15

[19] Penn S M, Beijers J P M, Dressler R A, Bierbaum V M and Leone S R 1990 Laser-induced fluorescence measurements of drift-velocity distributions for Ba + in Ar: moment

analysis and a direct measure of skewness *J. Chem. Phys.* **93** 5118–27

[20] Bastian M J, Lauenstein C P, Bierbaum V M and Leone S R 1993 Single frequency laser probing of velocity component correlations and transport properties of Ba^+ drifting in Ar *J. Chem. Phys.* **98** 9496–512

[21] Foerste M, Guenther H, Riediger O, Wiebe J and Putlitz G Z 1998 Temperature dependent mobility measurements of alkali-earth ions in superfluid helium (^{4}He) *J. Low Temp. Phys.* **110** 231–6

[22] Mella M, Colombo M C and Morosi G 2002 Ground state and excitation dynamics in Ag doped helium clusters *J. Chem. Phys.* **117** 9695–702

[23] Abdessalem K, Mejrissi L, Issaoui N, Oujia B and Gadéa F X 2013 One and two-electron investigation of electronic structure for Ba^+Xe and BaXe van der Waals molecules in a pseudopotential approach *J. Phys. Chem.* A **117** 8925–38

[24] Abdessalem K, Mejrissi L, Habli H, Issaoui N, Ghalla H and Oujia B 2019 Spectroscopic and electric dipole properties of the Van der Waals interaction between barium and krypton atoms *Mol. Phys.* **117** 143–57

[25] Viehland L A and Hampt D S 1992 The distribution of velocities for Ba^+ ions in Ar gas *J. Chem. Phys.* **97** 4964–73

[26] Czuchaj E, Rebentrost F, Stoll H and Preuss H 1995 Pseudopotential calculations for the potential energies of LiHe and BaHe *Chem. Phys.* **196** 37–46

[27] Czuchaj E, Rebentrost F, Stoll H and Preuss H 1998 Calculation of ground-and excited-state potential energy curves for barium-rare gas complexes in a pseudopotential approach *Theor. Chem. Acc.* **100** 117–23

[28] Issa K, Abdessalem K, Issaoui N, Yaghmour S J, Ali K and Oujia B 2016 Theoretical study of Stability and Structure of $Ba^{2+}Ar_n$ (n = 1–25) Clusters *J. Mater. Environ. Sci.* **7** 889–98

[29] Abdessalem K, Habli H, Ghalla H, Yaghmour S J, Calvo F and Oujia B 2014 Many-body effects on the structures and stability of $Ba^{2+}Xe_n$ (n = 1–39, 54) clusters *J. Chem. Phys.* **141** 154308

[30] Tuttle W D, Harris J P, Zheng Y, Breckenridge W H and Wright T G 2018 Hybridization and Covalency in the Group 2 and Group 12 Metal Cation/Rare Gas Complexes *J. Phys. Chem.* A **122** 7679–703

[31] Bezrukov D S, Kleshchina N N, Kalinina I S and Buchachenko A A 2019 *Ab initio* interaction potentials of the Ba, Ba^+ complexes with Ar, Kr, and Xe in the lowest excited states *J. Chem. Phys.* **150** 064314

[32] Mtiri S and Oujia B 2019 Spectroscopic, vibrational and structural properties analysis of CaXen (n = 1–4) clusters *Comput. Theor. Chem.* **1151** 58–71

[33] Lovallo C C and Klobukowski M 2004 Accurate *ab initio* pair potentials between helium and the heavier group 2 elements *J. Chem. Phys.* **120** 246–52

[34] Mella M, Calderoni G and Cargnoni F 2005 Predicting atomic dopant solvation in helium clusters: The $Mg\,He_n$ case *J. Chem. Phys.* **123** 054328

[35] Czuchaj E, Rebentrost F, Stoll H and Preuss H 1993 Use of non-local l-dependent pseudopotentials in the calculation of the potential energies for the Ba-rare gas systems *Chem. Phys.* **177** 107–17

[36] Kleinekathöfer U 2000 Ground state potentials for alkaline-earth–helium diatoms calculated by the surface integral method *Chem. Phys. Lett.* **324** 403–10

[37] Lovallo C C and Klobukowski M 2003 Accurate *ab initio* alkaline earth–helium pair potentials *Chem. Phys. Lett.* **373** 439–47

[38] Mtiri S, Mejrissi L, Habli H, Al-Ghamdi A A, Oujia B and Gadéa F X 2017 Theoretical investigation of the diatomic Van der Waals systems Ca^+He and CaHe *Comput. Theor. Chem.* **1114** 33–46

[39] Bejaoui M, Dhiflaoui J, Mabrouk N, Berriche H and El Oualhazi R 2016 Theoretical investigation of the electronic structure and spectra of $Mg^{2+}He$ and Mg^+ He *J. Phys. Chem.* A **120** 747–53

[40] Dhiflaoui J, Bejaoui M, Farjallah M and Berriche H 2018 Investigation of the electronic structure of $Be^{2+}He$ and Be^+He, and static dipole polarisabilities of the helium atom *Mol. Phys.* **116** 1347–57

[41] Leung A W K, Julian R R and Breckenridge W H 1999 Potential curves for several electronic states of the MgHe, Mg^+He, and $Mg^{2+}He$ van der Waals complexes *J. Chem. Phys.* **111** 4999–5003

[42] Leung A W K and Breckenridge W H 1999 An *ab initio* study of the ground states and some excited states of BeRG, Be^+RG, and $Be^{2+}RG$ van der Waals complexes (RG = He, Ne) *J. Chem. Phys.* **111** 9197–202

[43] Sapse A-M, Dumitra A, Jain D C and Theoretical A 2003 Study of $LiHe_n^+$, $NaHe_n^+$, and $MgHe_n^+$ Complexes, with n = 1, 2, 3, 4 *J. Cluster Sci.* **14** 21–30

[44] Bu X and Zhong C 2004 *Ab initio* analysis of geometric structures of $BeHe_n^+$ (n = 1–12) clusters *Chem. Phys. Lett.* **392** 181–6

[45] Bu X, Zhong C and Jalbout A F 2004 *Ab initio* studies of MHe_n^+ (M = Be, Mg; n = 1–4) complexes *Chem. Phys. Lett.* **387** 410–4

[46] Mella M and Cargnoni F 2014 Exciplexes with ionic dopants: stability, structure, and experimental relevance of $M^+(^2Py)^4He_n$ (M = Sr, Ba) *J. Phys. Chem.* A **118** 6473–83

[47] Bu X and Zhong C 2005 Geometric structures and properties of $Mg^{m+}He_n$ (m = 1, 2; n = 1–10) clusters: *ab initio* studies *J. Mol. Struct.: THEOCHEM* **726** 99–105

[48] Page A J and von Nagy-Felsobuki E I 2008 *Ab initio* study of ground state MH_2, $HMHe^+$ and MHe_2^{2+}, M = Mg, Ca *Phys. Chem. Chem. Phys.* **10** 1285–91

[49] Andrejeva A, Gardner A M, Graneek J B, Breckenridge W H and Wright T G 2015 Theoretical Study of $M^+–RG_2$:(M^+ = Ca, Sr, Ba, and Ra; RG = He–Rn) *J. Phys. Chem.* A **119** 5995–6005

[50] MOLPRO version 2012.1, a package of *ab-initio* programs designed by Werner H-J *et al* (www.molpro.net)

[51] Woon D E and Dunning T H Jr 1994 Gaussian basis sets for use in correlated molecular calculations. IV. Calculation of static electrical response properties *J. Chem. Phys.* **100** 2975–88

[52] Lim I S, Stoll H and Schwerdtfeger P 2006 Relativistic small-core energy-consistent pseudopotentials for the alkaline-earth elements from Ca to Ra *J. Chem. Phys.* **124** 034107

[53] Hill J G and Peterson K A 2017 Gaussian basis sets for use in correlated molecular calculations. XI. Pseudopotential-based and all-electron relativistic basis sets for alkali metal (K–Fr) and alkaline earth (Ca–Ra) elements *J. Chem. Phys.* **147** 244106

[54] Brust J and Greene C H 1997 Theoretical investigation of barium-helium collisions. II. The excitation transfer cross sections *Phys. Rev.* A **56** 2013

[55] Mills I, Cvitaš T, Homann K, Kallay N and Kuchitsu K 1993 *Quantities, Units and Symbols in Physical Chemistry* (Oxford: Blackwell Science)

[56] Tang K T and Toennies J P 1984 An improved simple model for the van der Waals potential based on universal damping functions for the dispersion coefficients *J. Chem. Phys.* **80** 3726–41

[57] Yan Z C, Babb J F, Dalgarno A and Drake G W F 1996 Variational calculations of dispersion coefficients for interactions among H, He, and Li atoms *Phys. Rev.* A **54** 2824

[58] Müller W, flesh J and Meyer W 1984 Treatment of intershell correlation effects in abinitio calculations by use of core polarization potentials. Method and application to alkali and alkaline earth atoms *J. Chem. Phys.* **80** 3297–310

[59] Issaoui N, Abdessalem K, Ghalla H, Yaghmour S J, Calvo F and Oujia B 2014 Theoretical investigation of the relative stability of Na^+He_n (n = 2–24) clusters: Many-body versus delocalization effects *J. Chem. Phys.* **141** 174316

[60] Kramida A, Ralchenko Y, Reader J and N I S T A S D Team 2018 NIST Atomic Spectra Database (version 5.6.1) (https://physics.nist.gov/asd) [Mon Mar 18, 2019]. National Institute of Standards and Technology, Gaithersburg, MD (https://doi.org/10.18434/T4W30F)

[61] Jones J E and Ingham A E 1925 On the calculation of certain crystal potential constants, and on the cubic crystal of least potential energy *Proc. R. Soc.* A **107** 636

[62] Schwerdtfeger P, Gaston N and Krawczyk R P 2006 Extension of the Lennard-Jones potential: Theoretical investigations into rare-gas clusters and crystal lattices of He, Ne, Ar, and Kr using many-body interaction expansions *Phys. Rev.* B **73** 064112

[63] Wales D J and Doyle J P K 1997 Global optimization by basin-hopping and the lowest energy structures of Lennard-Jones clusters containing up to 110 atoms *J. Phys. Chem.* A **101** 5111–6

[64] Wales D J and Scheraga H 1999 Global optimization of clusters, crystals, and bio-molecules *Science* **285** 1368–72

[65] Gaied W, Habli H, Oujia B and Gadea F X 2011 Theoretical study of the MgAr molecule and its ion Mg^+Ar: potential energy curves and spectroscopic constants *Eur. Phys. J.* D **62** 371

[66] Bellert D and Breckenridge W H 2002 Bonding in Ground-State and Excited-State A^+Rg van der Waals Ions (A = Atom, Rg = Rare-Gas Atom): a Model-Potential Analysis *Chem. Rev.* **102** 1595–622

[67] Wang W J and Havey M D 1984 Near-ultraviolet emission bands of Li-rare-gas molecules *Phys. Rev.* A **29** 3184–8

[68] Lee C J and Havey M D 1990 Laser spectroscopy of the $3s\ ^2\Sigma^+ \leftarrow 2p\ ^2\Pi$ transition in LiNe *Phys. Rev.* A **43** 6066–74

[69] Davis S J, Rawlins W T, Galbally-Kinney K L and Kessler W J 2009 *Proc. of SPIE* (The Int. Society for Optical and Photonics) February vol 7196, p 71960G

[70] An der Lan L, Bartl P, Leidlmair C, Jochum R, Denifl S, Echt O and Scheier P 2012 Solvation of Na^+, K^+, and their dimers in helium *Chem. Eur. J.* **18** 4411–8

[71] Coccia E, Bodo E, Marinetti F, Gianturco F A, Yildirim E, Yurtsever M and Yurtsever E 2007 Bosonic helium droplets with cationic impurities: onset of electrostriction and snowball effects from quantum calculations *J. Chem. Phys.* **126** 124319

[72] Marinetti F, Coccia E, Bodo E, Gianturco F A, Yurtsever E, Yurtsever M and Yildirim E 2007 Bosonic helium clusters doped by alkali metal cations: interaction forces and analysis of their most stable structures *Theor. Chem. Acc.* **118** 53

[73] Di Paola C, Sebastianelli F, Bodo E, Baccarelli I, Gianturco F A and Yurtsever M 2005 Microsolvation of Li^+ in small he clusters. Li^+He_n species from classical and quantum calculations *J. Chem. Theory Comput.* **1** 1045–54

[74] Sebastianelli F, Bodo E, Baccarelli I, Di Paola C, Gianturco F A and Yurtsever M 2006 Microsolvation of Li^+ in bosonic helium clusters. I. Many-body effects on the structures of the small aggregates *Comput. Mater. Sci.* **35** 261–7

[75] Ambrosetti A, Ferri N, DiStasio R A Jr and Tkatchenko A 2016 Wavelike charge density fluctuations and van der Waals interactions at the nanoscale *Science* **351** 1171

[76] Ambrosetti A and Silvestrelli P L 2018 Hidden by graphene - towards effective screening of interface van der Waals interactions via monolayer coating *Carbon* **139** 486

[77] Mtiri S, Laajimi M, Ghalla H and Oujia B 2020 Microsolvation of Ca^{2+} cation in small Xe_n clusters: Structures and relative stabilities *Physica.* B **578** 411849

[78] Lüder C, Prekas D and Velegrakis M 1997 Ion-size effects in the growth sequences of metal-ion-doped noble gas clusters *Laser Chem.* **17** 109–22